第 2 卷　第 5 期
2013 年 9 月

集　成　技　术
JOURNAL OF INTEGRATION TECHNOLOGY

Vol. 2　No. 5
Sep. 2013

开放式的高分辨率超声成像系统

邱维宝[1]　于妍妍[2]　黎国锋[1]　钱　明[1]　孙　雷[2]　郑海荣[1]*

[1]（中国科学院深圳先进技术研究院生物医学与健康工程研究所　深圳　518055）

[2]（香港理工大学物医学工程跨领域学部　香港）

摘　要　在医学和生物学研究当中，对活体组织进行无创性成像具有重要意义。高分辨率超声成像技术，可以对细微组织实现高空间分辨率的成像，已被广泛应用于皮肤、眼睛、心血管和小动物成像等生物医学领域。目前领域内的相关研究需要不同的成像系统参数，例如要求不同的探头性能、数据采集策略、信号处理以及图像重建、显示和保存方法。因此需要一种灵活和开放的超声成像系统，能让用户根据各种研究需求实现个性化设置并能全面获取原始实验数据。文章提出了一种实时的、便携式设计的开放式超声成像系统，可支持定制的高分辨率超声成像研究。系统基于高速现场可编程逻辑门阵列(FPGA)实现灵活多样的超声成像。用户可以轻松地根据个性化应用需求来调整系统结构。测试结果表明，本系统能实现 B 超成像、编码激励成像、多普勒成像、血管内成像、多模态组合成像等，为高分辨率生物医学应用研究提供了非常灵活的成像工具。

关键词　超声成像；高分辨率成像；开放式系统；可编程逻辑阵列；实时成像

Open System for High Resolution Ultrasound Imaging

QIU Wei-bao[1]　YU Yan-yan[2]　LI　Guo-feng[1]　QIAN Ming[1]　SUN Lei[2]　ZHENG Hai-rong[1]*

[1](Institute of Biomedical and Health Engineering, Shenzhen Institutes of Advanced Technology,

Chinese Academy of Sciences, Shenzhen 518055, China)

[2](Interdisciplinary Division of Biomedical Engineering, The Hong Kong Polytechnic University, Hong Kong SAR, China)

Abstract　Noninvasive visualization of living tissues is in great demand in the field of medical and biological studies. High resolution ultrasound imaging has made it possible to image small structures with fine spatial resolution and been widely used in the biomedical field including the dermatology, ophthalmology, intravascular imaging, and small animal imaging. The individual study is unique in nature and requires different utilization of the imaging system, such as different transducer characteristics, data acquisition strategies, signal processing methods, and image reconstruction, display and storage. Therefore, there is a demand for a flexible and open imaging system to allow users to customize the system for various studies and have full access to experimental data. In this paper, a real-time compact and open system is developed for customized high resolution ultrasound imaging studies. The system was based on high-speed field programmable gate array (FPGA) embedded in compact printed circuit board (PCB) to achieve flexible ultrasound imaging. The system structure could easily be modified by the users for customized applications. Testing results show that the system can offer a very flexible setting with B-mode imaging, modulated excitation imaging, Doppler imaging, intravascular imaging, and multi-modality imaging for high resolution biomedical applications.

Keywords　ultrasound; high resolution imaging; open system; FPGA; real-time imaging

1 Introduction

High-resolution, noninvasive visualization of living tissues is an indispensable technique to observe physiological activities on a miniature scale. Diseases associated with small human structures such as eye, skin, blood vessel can benefit from this technique. In addition, this technique can also facilitate preclinical researches of small animal models of human diseases in mice, rats, zebrafish, etc. Preclinical studies of small animal models can improve the knowledge and understanding of physiological and functional mechanism of pathologies and treatment strategies. Current high-resolution imaging modalities include micro-CT (computed tomography)[1], micro-MRI (magnetic resonance imaging)[2], micro-PET (positron emission tomography)[3], optical coherent tomography (OCT)[4], and high-resolution ultrasound imaging[5-6].

High-resolution ultrasound imaging, also known as micro-ultrasound (micro-US) or ultrasound biomicroscope (UBM), has made it possible to delineate small structures with fine spatial resolution on the order of tens of microns[7]. It is clinically used for ophthalmology[8], dermatology[9], and intravascular diseases[10]. Preclinical small animal model research has also been significantly propelled by this technique, for example, malignant tumor diagnosis[11-12], cardiac diseases[13-14], and embryonic developmental biology[15-16]. Recently, it has been combined with optical method such as OCT or fluorescence spectroscopy as a dual-modality imaging technique and demonstrated great potentials in biomedical studies[17-19]. Other advanced imaging techniques also take the advantage of high-resolution ultrasound imaging and extend its biomedical investigations such as photoacoustic imaging[20-21], contrast enhanced imaging [22], modulated excitation imaging[23], 3D imaging[24], elastography imaging[10,25], and harmonic imaging[26]. Each study is unique in nature and requires different utilization of the ultrasound imaging system. Imaging systems(eg: vevo 770, vevo 2100, Visualsonics, Inc., Canada) with fixed specifications, such as transducer characteristics, data acquisition strategy, signal processing method, and image display approach, do not satisfy extensive preclinical study requirements. Researchers need a highly flexible device to best suit their specific investigations. In addition, access to the raw experimental data is also important to scientific discovery. Therefore, an open and flexible ultrasound imaging system allowing users/researchers to customize for individual biomedical study is necessary.

In this paper, the development of an open imaging system with high flexibility and compactness was described to satisfy various biomedical investigations. This open system incorporated a high-voltage arbitrary waveform generator, a programmable imaging receiver, high-precision servo motors, and high-performance transducers. FPGA was served as the core processor and replaced hardware circuitry for fast processing speed and programmability. Moreover, low-noise and high-speed analog electronics was used to achieve high signal-to-noise ratio (SNR) and high sensitivity. A PCIE bus, as a high-speed data transmission interface, was incorporated in this platform for image data or RF raw data transfer to a computer through direct memory access (DMA) operation. Nevertheless, all the electronics such as amplifier, filter, analog-to-digital converter (ADC) and FPGA were incorporated in a single PCB for compactness and cost-effectiveness. It was demonstrated that B-mode imaging, Doppler imaging, modulated excitation imaging, and intravascular imaging were realized in this system.

2 System Description

The designed open system included a high-frequency pulse generator, a high-speed ultrasound imaging receiver with analog front-end electronics and digital back-end unit, and a high-speed mechanical scan probe. The block diagram is shown in Fig.1. The pulse generator employed FPGA and high-speed metal-oxide-semiconductor field effect transistors (MOSFETs) to achieve high-voltage pulse generation. A high-speed imaging receiver was developed including front-end electronics, ADC, FPGA, and high-speed computer interfaces, which allowed to process the images in real-time with high programmability and flexibility. A personal computer was employed for image display and data storage for further investigations.
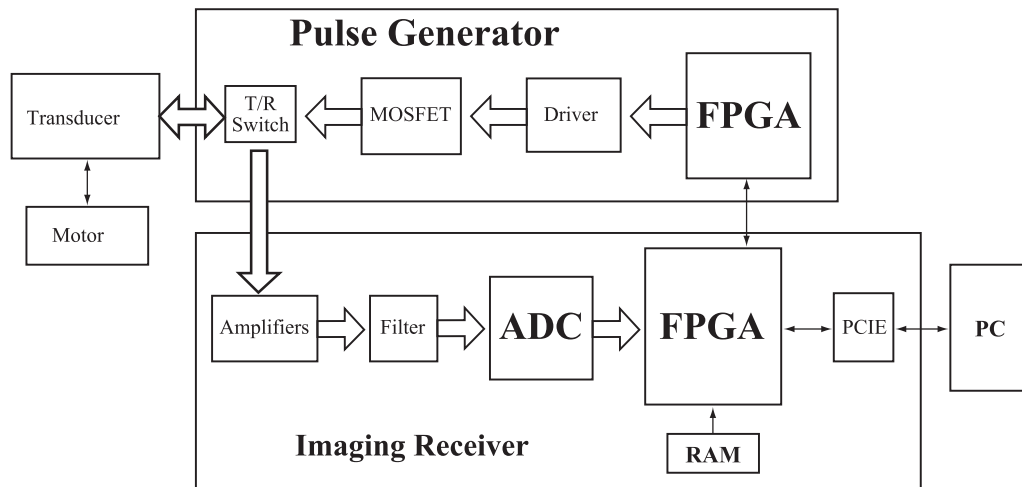
Figure 1.　The block diagram of the high-resolution open system

Graphical user interface software was programmed in Visual C++ to process real-time ultrasound images. A PCIE bus utilization supports high-speed data transfer and real-time imaging.

2.1　Pulse Generator

The designed pulse generator for this open system incorporated a bipolar pulse generation scheme and an arbitrary waveform generator. A programmable FPGA component (Cyclone III, EP3C16F484C6N, Altera Corporation, San Jose, CA) was employed to control the timing and spectrum characteristics of the high voltage short pulse. Therefore, the pulse generator could be easily adjusted to support transducers with different center frequencies as well as match with the spectrum of individual transducer to acquire the optimized performance. Two MOSFET drivers (EL7158, Intersil Corporation, Milpitas, CA) were employed to accomplish the voltage level shift and high current output to excite the high-speed MOSFET pair (TC6320, Supertex Inc., Sunnyvale, CA). The MOSFET pair could offer more than 150 Vpp breakdown voltages and a 2A output peak current, which made it suitable to produce a high-voltage pulse for ultrasound imaging.

　The waveform for modulated excitation imaging usually requires amplitude and frequency modulation (Chirp excitation) or phase modulation (Barker excitation and Golay excitation) of sinusoidal carrier signal. A programmable high-voltage arbitrary waveform generator was designed to generate various arbitrary waveforms for different modulated excitation imaging. A 16-bit DAC (DAC5682Z, Texas Instruments Inc., TX) with 1 giga-samples per second (GSPS) was employed to convert digital arbitrary waveforms to analog signals at a frequency higher than 100 MHz. Two stages of high-speed operational amplifiers (THS3091, Texas Instruments Inc., TX) were used to amplify the waveforms. Then a push-pull vertical diffused metal-oxide-semiconductor (VDMOS) transistor (SR705, Polyfet RF Devices, Camarillo, CA) was employed in the third stage for high-voltage amplification.

2.2　High-speed Digital Receiver

The center frequency of high-resolution ultrasound is usually from 20 MHz to 80 MHz. So the echo receiver should have the capability to process this high-frequency ultrasound signal. In the developed open system, high-precision ultrasound signal amplification and acquisition, real-time image processing, and fast data transfer were achieved in the high-speed imaging receiver. It utilized low-noise amplifiers and high-speed ADC to amplify and digitize the small ultrasound echo signal, respectively. Raw RF data which were acquired by the ADC after low-noise amplification were processed directly by the high-speed FPGA for fast imaging and compact implementation. In detail, a low-noise amplifier (SMA231, Tyco Electronics Co., Berwyn, PA) was used as the first stage amplifier to support 27 dB gain. A low-distortion amplifier (THS4509, Texas Instruments Inc., Dallas, TX) was used as the second stage amplifier for further 20 dB amplification. A low-pass filter (RLP83+, Mini-Circuits, Brooklyn, NY) with a cut frequency of

93 MHz was employed for ADC anti-aliasing. A high-speed 11 bits ADC (ADS5517, Texas Instruments Inc., Dallas, TX) with a maximum sampling rate of 200 MSPS was utilized for data converting. After the digitization, the digital signal was transferred to FPGA through the low-voltage differential signaling (LVDS) bus. A high-performance FPGA (Stratix II EP2S60F672I4, Altera Corporation, San Jose, CA) with great signal integrity was employed, which could support data processing at an adequate speed. This component included 39 DSP blocks (total 288 9×9Multipliers) which could efficiently implement high-speed digital signal processing algorithms. It demonstrated up to 287 MHz high order FIR, Hilbert transform and high-speed DSC algorithms. It could also support DDR2 SDRAM and PCI interface. A 512M bits RAM combined with two DDR2 SDRAM (MT47H16M16, Micron Technology Inc., Boise, ID) was used for temporary buffering of data. Various programmable algorithms could be achieved in the FPGA including band pass filter, compression filter, envelope detector, and digital scan converter for modulated excitation imaging. The receiver also supported raw RF data acquisition. Both processed image data and raw RF data could be transferred to a computer through PCIE interface (PEX8311, PLX Technology Inc, Sunnyvale, CA) for displaying or post-processing.

2.3　Imaging Algorithms

As a field programmable microprocessor, the FPGA can achieve various functionalities traditionally realized by hardware circuitry. Moreover, the functions could easily be changed or modified by reprogramming the FPGA without change of hardware. Thus, the FPGA technology could significantly improve the system flexibility and diversity by programmable and reconfigurable algorithms.

Fig. 2 shows the representative structure of implemented algorithms for real-time B-mode imaging and directional PW Doppler.

For B-mode imaging, three steps were adopted for data preconditioning, i.e. in the order of execution, band pass filter (BPF), digital time gain compensation (TGC) and envelope detection. After removing noises by BPF, the data were digitally amplified by configurable coefficients to compensate for ultrasound attenuation loss in tissues called TGC. The acquired envelop data then underwent DSC and logarithmic compression. The TGC, DSC and logarithm compressor were all reconfigurable by users through GUI software. For directional PW Doppler, BPF was also employed but with different coefficients configuration tuned for flow measurement. A novel digital quadrature demodulation was used to extract the flow information from the echo signal. The data were then saved in the dual port RAM for gate selection. When a train of data was accumulated, the spectrum extraction was then launched to estimate the flow velocity. Finally, image data or spectrogram data were sent to a computer through PCIE bus for display and storage.

2.4　Evaluation Method

The performance of the open system electronics was tested by a 240 MHz function generator (AFG 3251, Tektronix Inc., Beaverton, OR), a digital oscilloscope (LeCroy wavepro 715Zi, LeCroy Corp., Chestnut Ridge, NY), a signal generator (HP8656B, Hewlett Packard), a spectrum analyzer (HP8591E, Hewlett Packard), and a series of attenuators (Mini-Circuits, Brooklyn, NY). The signal generator and the spectrum analyzer were employed to test the gain linearity and flatness of analog electronics. The noise level of the system was tested by measuring the minimum detectable signal level and
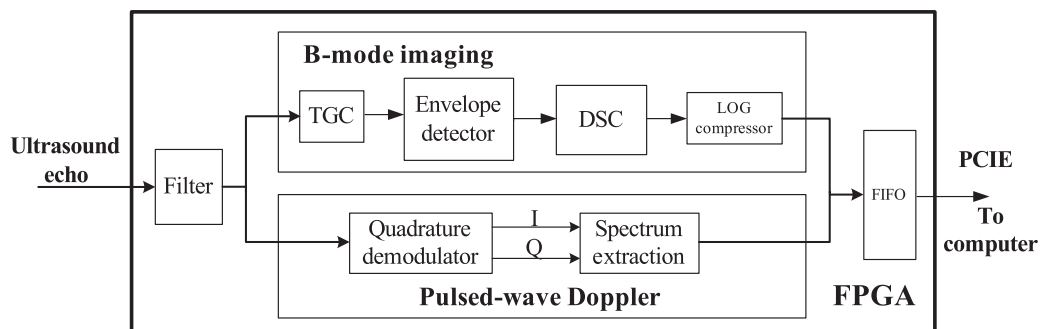

Figure 2.　Schematic of algorithms implemented in the FPGA for real-time B-mode imaging and directional pulsed-wave Doppler.

dynamic range. Five-cycle sinusoidal signal generated by the function generator was attenuated by a series of attenuators and then sent to the imaging receiver. After passing through the front-end electronics, the amplitude of the weak signal that could just be identified from the background noise determined the minimum detectable signal level. Given the input range of the high-speed ADC (2 Vpp), the dynamic range could be derived from the gain and the minimum detectable signal level.

　　A wire phantom consisting of five 20 μm diameter tungsten wires (California Fine Wire Co., CA), was used to evaluate the image resolution. A tissue mimicking phantom was fabricated to further test the image quality of the open platform. The phantom fabrication procedure followed Madsen's method[27]. It consisted of a mixture of deionized water, high-grade agarose, preservative, propylene glycol, filtered bovine milk, and glass-bead to generate tissue mimicking attenuation and backscattering. Anechoic spheres were fabricated separately and dispersed in the phantom to test the system resolution. The size of the anechoic spheres was in the range of 180-280 μm controlled by a dedicated sieve (Fisherbrand sieves, Fisher Scientific, Pittsburgh, PA).

3　Results

The system prototype for the proposed open system was shown in Fig. 3. Fig. 3(a) showed the arbitrary waveform generator in an eight-layer PCB. Fig. 3(b) showed the programmable imaging receiver with an eight-layer PCB incorporating low-noise front-end electronics, ADC, SDRAM, high speed FPGA, and PCIE interface.

3.1　Electronics Performance

Table 1 summarized the performance of the open system electronics. The highest amplitude of bipolar pulse was 160 Vpp with adjustable center frequency and bandwidth (Fig. 4). Table 1 also demonstrates that the maximum gain of the front-end electronics is 47 dB with good linearity at a maximum fluctuation of less than ±1.2 dB between 10 MHz and 90 MHz. The minimal detectable signal level of the system receiver is less than 25 μV. Given the input range of the high-speed ADC (2 Vpp), the system can allow a 51 dB dynamic range at 35 MHz center

(a)

(b)

Figure 3.　(a)Photographs of the designed open system including a programmable pulse generator (b) and a high-speed imaging receiver

frequency.

　　The software-based band pass filter (BPF) was programmed in the FPGA to further remove the noise and improve the signal SNR. Quantitative analysis showed that approximately 4.8 dB SNR improvement was achieved after applying the BPF, which increased the system dynamic range to 55.8 dB. The algorithmic scheme implemented in the FPGA could achieve high-speed imaging by pipe-line signal processing. The data transferring speed was higher than 150 MByte/s for PCIE interface. At the image size of 512×512 pixels, the frame rate can be higher than 200 images per second for PCIE. Current frame rate is limited by the motor, and it can be

Table 1.　Electronics performance of the open system

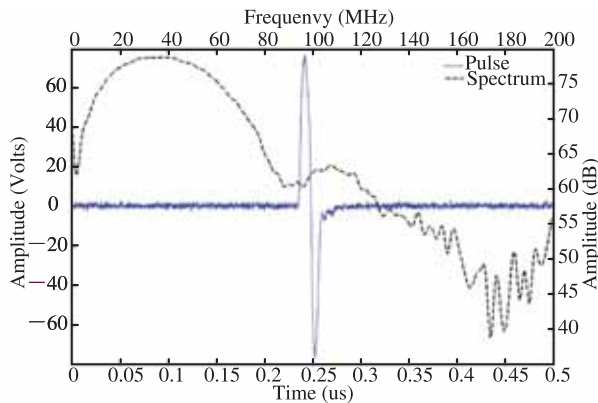| Articles	Performance
Frequency range	$20-80$ MHz
High-voltage tunable pulse	Up to 160 Vpp
Gain	47 dB
Gain fluctuation	±1.2 dB
ADC	11 bits, 200 MSPS
Minimum detectable signal	25 μV
Dynamic range	51 dB
Improved dynamic range	55.8 dB
Data transferring speed	150 MByte/s

Figure 4.   High-voltage bipolar monocycle pulse with 35 MHz center frequency, 150 Vpp amplitude, and 56 MHz 6dB bandwidth.

significantly improved if a faster motor is used. With the current utilization of FPGA resources, much more complicated signal processing may be implemented to acquire useful information than vessel morphology, such as the virtual histology (tissue characterization based on ultrasound raw RF data).

3.2   B-mode Imaging

The image quality of this system was evaluated by a customized wire phantom. The wire phantom consisted of five 20 μm diameter tungsten wires (California Fine Wire Co., CA) of which distance intervals along vertical and horizontal directions were 1.6 mm and 1.0 mm respectively. The ultrasound image of this wire phantom was shown in Fig. 5 with a dynamic range of 50 dB. In this experiment, a 35 MHz PVDF single element transducer was employed. (Characteristics: focal length 13.6 mm, bandwidth 88%, f-number 2.7). No visible noise was noticed in this image.

Fig. 6 showed the ultrasound image of the tissue phantom acquired by this system prototype. The black circular dots appearing in the images were the anechoic spheres producing no detectable echoes. The diameter of the spheres were at approximately 180 μm, correlating well with the actual sphere size. The transducer for this experiment was a 50 MHz lithium niobate (LiNbO$_3$) transducer with focal length of 9.3 mm and bandwidth of 47%.

3.3   Flow Imaging

Fig. 7 showed an in vivo spectrogram acquired from a vein in the back of a human hand. A needle transducer (42.5 MHz) was placed close to the vein coupled by ultrasound gel with an angle of 72 degrees approximately.
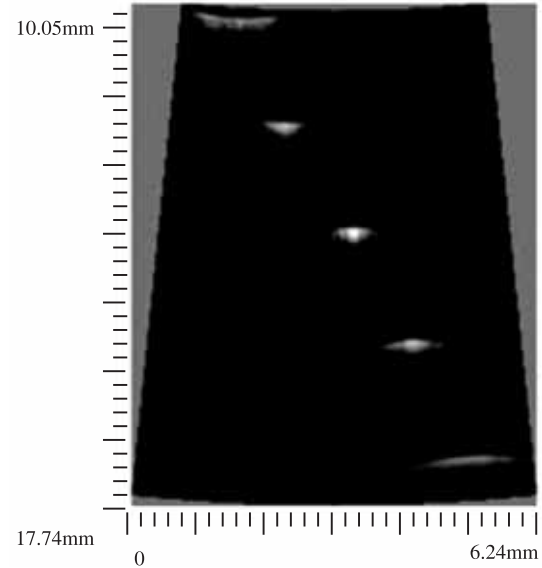

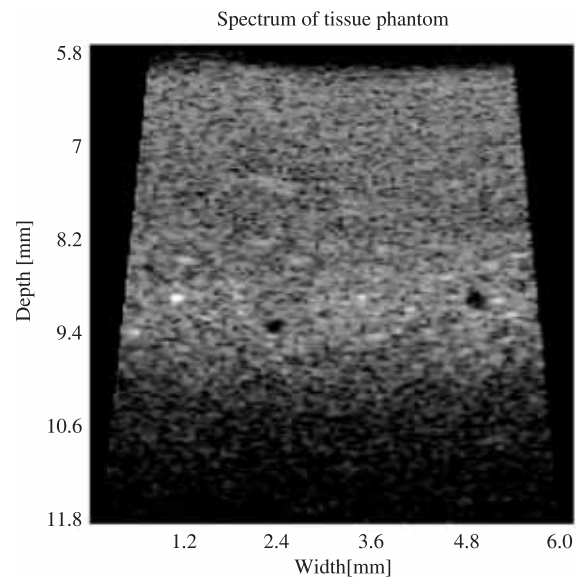Figure 5.   Wire phantom image of the open platform.

Figure 6.   Image of tissue phantom with anechoic spheres. The dynamic range for this test is set at 48 dB. The trigger pulse is single cycle 150 Vpp bipolar pulse.
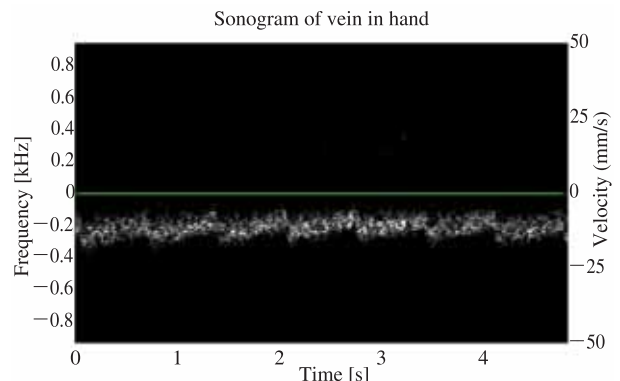

Figure 7.   The pulsed-wave Doppler waveform of a vein in the back of a human hand.

A seven-cycle 40Vpp sinusoidal pulse was generated with PRF of 1.95 KHz. The blood moving away from the transducer confirmed the negative velocity profile. The cyclic pattern of the spectrogram correlated well to the heart beat of the subject. The heart rate was 80 beats/min measured from the spectrogram agreed with the heart rate of 78 beats/min of the subject.

3.4 Modulated Excitation Imaging

Fig. 8 showed in vivo ultrasound images of the dorsal skin of a human hand acquired by the short pulse imaging and the modulated excitation imaging with the proposed system. The dynamic range was set to 52 dB in both two images. The image of modulated excitation was brighter than the image of short pulse excitation, simply because the echo signals from the modulated excitation method was much larger. The penetration depth has been significantly improved by the chirp-based modulated excitation imaging technique. Moreover, motor noise was clearly visible in the short pulse imaging, while the noise was unnoticeable in the modulated excitation imaging.
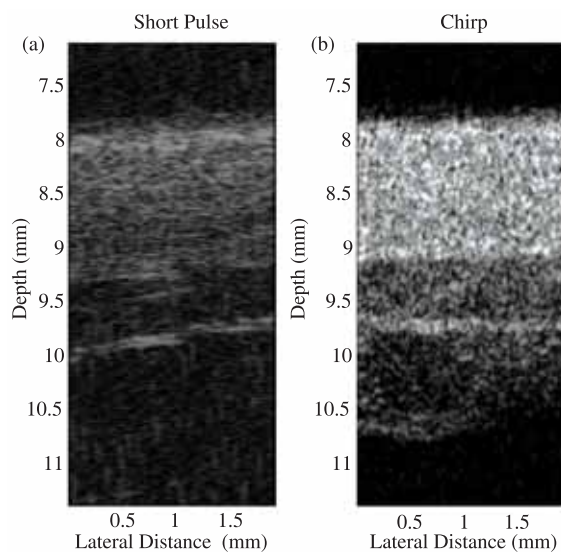

Figure 8. *In vivo* images of the dorsal skin of a human hand
(a) The image of short pulse imaging. (b) The image of chirp-based
modulated excitation imaging.

3.5 Intravascular Imaging

The designed open system supports various applications for micro-ultrasound techniques. Intravascular ultrasound imaging was also achieved by replacing the transducer with IVUS transducer. The motor was also changed with a rotary motor. In vitro coronary artery specimen was used for system evaluation. The ultrasound image of

specimen was shown in Fig. 9(a). Different layers of the artery could be clearly identified in the ultrasound image. The result from a multi-modality imaging combining IVUS and photoacoustics was shown in Fig. 9(b). An actively Q-switched pulsed laser (Explorer 532 Laser System, Spectra-Physics, Santa Clara, CA) operating at 532 nm wavelength generated very short laser pulses with 240 μJ energy. Ultrasound imaging was launched after the acquisition of photoacoustic signal. The echo intensity of ultrasound imaging slightly increased in bottom right corner of the tissue. This difference could be clearly visualized in photoacoustic image which indicated the change of tissue composition. Combined image showed the complementary nature of ultrasound imaging and photoacoustic imaging that could be useful for the diagnosis of intravascular diseases. This in vitro experimental result clearly demonstrated the capability and flexibility of the proposed open system.
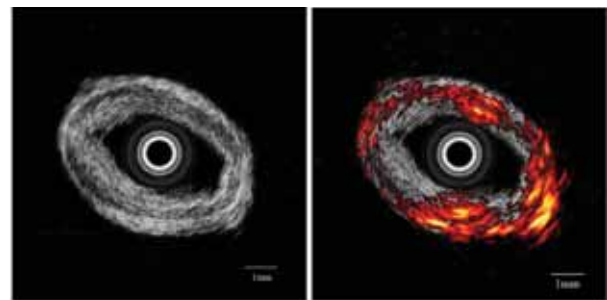

Figure 9. *In vitro* imaging of human coronary artery (a) IVUS image.
(b) Combined image of IVUS and photoacoustics.

4 Conclusions

In this paper, a programmable open system for real-time high-resolution ultrasound was developed and evaluated based on a high-speed FPGA. It was implemented in a compact and cost-effective PCB scheme. This open system demonstrated a high image quality with a good spatial resolution for preclinical small animal imaging. The flexible and programmable design makes the open system suitable for various biomedical studies.

References

[1] Badea C T, Drangova M, Holdsworth D W, et al. In vivo small animal imaging using micro-CT and digital subtraction

angiography [J]. Physics in Medicine and Biology, 2008, 53(19): 319-350.

[2]　Driehuys B, Nouls J, Badea A, et al. Small animal imaging with magnetic resonance microscopy [J]. ILAR Journal, 2008, 49(1): 35-53.

[3]　Schnöckel U, Hermann S, Stegger L, et al. Small-animal PET: a promising, non-invasive tool in pre-clinical research [J]. European Journal of Pharmaceutics and Biopharmaceutics, 2010, 74(1): 50-54.

[4]　Fujimoto J G. Optical coherence tomography for ultrahigh resolution in vivo imaging [J]. Nature Biotechnology, 2003, 21(11): 1361-1367.

[5]　Foster F S, Zhang M Y, Zhou Y Q, et al. A new ultrasound instrument for in vivo microimaging of mice [J]. Ultrasound in Medicine and Biology, 2002, 28(9): 1165-1172.

[6]　Foster F S, Mehi J, Lukacs M, et al. A new 15-50 MHz array-based micro-ultrasound scanner for preclinical imaging [J]. Ultrasound in Medicine and Biology, 2009, 35(10): 1700-1708.

[7]　Foster F S, Pavlin C J, Harasiewicz K A, et al. Advances in ultrasound biomicroscopy [J]. Ultrasound in Medicine and Biology, 2000, 26(1): 1-27.

[8]　Silverman R H, Ketterling J A, Coleman D J. High-frequency ultrasonic imaging of the anterior segment using an annular array transducer [J]. Ophthalmology, 2007, 114(4): 816-822.

[9]　Vogt M, Ermert H. In vivo ultrasound biomicroscopy of skin: spectral system characteristics and inverse filtering optimization [J]. IEEE Transactions on Ultrasonics, Ferroelectrics, and Frequency Control, 2007, 54(8): 1551-1559.

[10]　de Korte C L, van der Steen A F, Cespedes E I, et al. Characterization of plaque components and vulnerability with intravascular ultrasound elastography [J]. Physics in Medicind and Biology, 2000, 45(6): 1465-1475.

[11]　Cheung A M, Brown A S, Hastie L A, et al. Three-dimensional ultrasound biomicroscopy for xenograft growth analysis [J]. Ultrasound in Medicine and Biology, 2005, 31(6): 865-870.

[12]　Goessling W, North T E, Zon L I. Ultrasound biomicroscopy permits in vivo characterization of zebrafish liver tumors [J]. Nature Methods, 2007, 4(7): 551-553.

[13]　Zhou Y Q, Foster F S, Nieman B J, et al. Comprehensive transthoracic cardiac imaging in mice using ultrasound biomicroscopy with anatomical confirmation by magnetic resonance imaging [J]. Physiological Genomics, 2004, 18(2): 232-244.

[14]　Du J, Zhang C, Liu J, et al. A point mutation (R192H) in the C-terminus of human cardiac troponin I causes diastolic dysfunction in transgenic mice [J]. Archives of Biochemistry and Biophysics, 2006, 456(2): 143-150.

[15]　Zhou Y Q, Foster F S, Qu D W, et al. Applications for

multifrequency ultrasound biomicroscopy in mice from implantation to adulthood [J]. Physiological Genomics, 2002, 10(2): 113-126.

[16]　Kulandavelu S, Qu D, Sunn N, et al. Embryonic and neonatal phenotyping of genetically engineered mice [J]. ILAR Journal, 2006, 47(2): 103-117.

[17]　Römer T J, Brennan III J F, Puppels G J, et al. Intravascular ultrasound combined with Raman spectroscopy to localize and quantify cholesterol and calcium salts in atherosclerotic coronary arteries [J]. Arteriosclerosis, Thrombosis, and Vascular Biology, 2000, 20(2): 478-483.

[18]　Sun Y, Park J, Stephens D N, et al. Development of a dual-modal tissue diagnostic system combining time-resolved fluorescence spectroscopy and ultrasonic backscatter microscopy [J] Review of Scientific Instruments, 2009, 80(6): 065104.

[19]　Yang H C, Yin J, Hu C, Cannata J, et al. A dual-modality probe utilizing intravascular ultrasound and optical coherence tomography for intravascular imaging applications [J]. IEEE Transactions on Ultrasonics, Ferroelectrics, and Frequency Control, 2010, 57(12): 2839-2843.

[20]　Wang L V. Multiscale photoacoustic microscopy and computed tomography [J]. Nature Photonics, 2009, 3(9): 503-509.

[21]　Sethuraman S, Amirian J H, Litovsky S H, et al. Spectroscopic intravascular photoacoustic imaging to differentiate atherosclerotic plaques [J]. Optics Express, 2008, 16(5): 3362-3367.

[22]　Goertz D E, Cherin E, Needles A, et al. High frequency nonlinear B-scan imaging of microbubble contrast agents [J]. IEEE Transactions on Ultrasonics, Ferroelectrics, and Frequency Control, 2005, 52(1): 65-79.

[23]　Mamou J, Aristizábal O, Silverman R H, et al. High-frequency chirp ultrasound imaging with an annular array for ophthalmologic and small-animal imaging [J]. Ultrasound in Medicine and Biology, 35(7): 1198-1208.

[24]　Wirtzfeld L A, Wu G, Bygrave M, et al. A new three-dimensional ultrasound microimaging technology for preclinical studies using a transgenic prostate cancer mouse model [J]. Cancer Research, 2005, 65(14): 6337-6345.

[25]　Maurice R L, Daronat M, Ohayon J, et al. Non-invasive high-frequency vascular ultrasound elastography [J]. Physics in Medicine and Biology, 2005, 50(7): 1611-1628.

[26]　Needles A, Arditi M, Rognin N G, et al. Nonlinear Contrast Imaging with an Array-Based Micro-Ultrasound System [J]. Ultrasound in Medicine and Biology, 2010, 36(12): 2097-2106.

[27]　Madsen E L, Frank G R, McCormick M M, et al. Anechoic sphere phantoms for estimating 3-D resolution of very-high-frequency ultrasound scanners [J]. IEEE Transactions on Ultrasonics, Ferroelectrics, and Frequency Control, 2010, 57(10): 2284-2292.